



Nabro volcano aerosol in the stratosphere from twilight spectrometry

N. Mateshvili et al.

This discussion paper is/has been under review for the journal Atmospheric Measurement Techniques (AMT). Please refer to the corresponding final paper in AMT if available.

Nabro volcano aerosol in the stratosphere over Georgia, South Caucasus from ground-based spectrometry of twilight sky brightness

N. Mateshvili^{1,2}, D. Fussen¹, G. Mateshvili², I. Mateshvili², F. Vanhellemont¹, E. Kyrölä³, S. Tukiainen³, J. Kujanpää³, C. Bingen¹, C. Robert¹, C. Tétard¹, and E. Dekemper¹

¹Belgian Institute for Space Aeronomy, Brussels, Belgium

²Abastumani Astrophysical Observatory, Ilia State University, Georgia

³Finnish Meteorological Institute, Helsinki, Finland

Received: 18 March 2013 – Accepted: 26 April 2013 – Published: 17 May 2013

Correspondence to: N. Mateshvili (ninam@aeronomie.be)

Published by Copernicus Publications on behalf of the European Geosciences Union.

Title Page	
Abstract	Introduction
Conclusions	References
Tables	Figures
◀	▶
◀	▶
Back	Close
Full Screen / Esc	
Printer-friendly Version	
Interactive Discussion	



Abstract

Ground-based spectral measurements of twilight sky brightness were carried out between October 2009 and August 2011 in Georgia, South Caucasus. The algorithm which allowed to retrieve the lower stratospheric and upper tropospheric aerosol extinction profiles was developed. The Monte-Carlo technique was used to correctly represent multiple scattering in a spherical atmosphere. The estimated stratospheric aerosol optical depths at a wavelength of 780 nm were: $3.0 \times 10^{-3} \pm 1 \times 10^{-3}$ (31 August 2009–15 January 2011) and $1.1 \times 10^{-2} \pm 3 \times 10^{-3}$ (18 July 2011–03 August 2011, 10 observations). The first optical depth value corresponds to the background stratospheric aerosol level, the last one to the volcanically disturbed one after the Nabro eruption in June 2011.

Reconsideration of measurements acquired soon after the Pinatubo eruption in 1991 allowed to model the phenomenon of the “second purple light”, a twilight sky brightness enhancement at large solar zenith angles (97–102°). Monte-Carlo modeling reveals that the second purple light is caused by multiple scattering in the stratospheric aerosol layer.

The modeling also shows that, assuming a hypothetical mesospheric aerosol layer with optical extinction comparable to typical noctilucent cloud values, a measurable twilight sky brightness increase at wavelength 440 nm follows at solar zenith angles 98–99°.

1 Introduction

Stratospheric and upper tropospheric aerosols are important atmospheric constituents. They play an essential role in climate evolution because they influence the radiative balance and the global chemistry (e.g., Hendricks et al., 1999; Ramachandran et al., 2000). Volcanic eruptions inject large amounts of sulfur dioxide into the stratosphere where it is oxidized in presence of water into sulfuric acid that condensates into sulfuric

AMTD

6, 4401–4444, 2013

Nabro volcano aerosol in the stratosphere from twilight spectrometry

N. Mateshvili et al.

Title Page

Abstract

Introduction

Conclusions

References

Tables

Figures

⏪

⏩

◀

▶

Back

Close

Full Screen / Esc

Printer-friendly Version

Interactive Discussion



acid droplets forming the stratospheric aerosol layer (SAL). The last major event was the Mount Pinatubo eruption in 1991 which produced a large quantity of sulfur dioxide that strongly enhanced the SAL. After this eruption, the SAL decayed to its background condition within a few years (e.g., Baumann et al., 2003).

5 Long-duration time series of both satellite-based and ground based stratospheric aerosol measurements analysis allowed Solomon et al. (2011), to conclude that the global stratospheric aerosol optical depth increased in 2000–2010 with about 7 % per year after a minimum was reached in 1998–2000. They estimated that the global radiative forcing decreased by about 1 W m^{-2} due to the increase of stratospheric aerosol
10 levels. During the same period the carbon dioxide content growth led to an increase of radiative forcing of 0.28 W m^{-2} (Solomon et al., 2011). The authors conclude that the background SAL variations make a significant contribution to the forcing change and hence climate change.

In absence of major eruptions the SAL load is fed by minor volcanic eruptions (Van-
15 hellefont et al., 2010; Vernier et al., 2011a) and possibly by anthropogenic sources (Brock et al., 2005; Hofmann et al., 2009; Vernier et al., 2011b).

SAL enhancements due to minor volcanic eruptions were routinely detected using different techniques during the last decade. Vanhellefont et al. (2010) presented an overview of the aerosol extinction profile retrievals for the GOMOS star occultation in-
20 strument, covering the period from August 2002 to May 2008. Elevated aerosol levels were detected in the second half of 2006 and 2007 after the eruption of the Soufrière Hills volcano on 20 May 2006. Bourassa et al. (2010) presented SAL monitoring results using limb measurements by the OSIRIS instrument on board the Odin satellite. The measurements that covered the period after the eruptions of Mount Okmok and
25 Kasatochi volcanos in 2008 allowed to retrieve vertical profiles of the stratospheric aerosol extinction. Hoffmann et al. (2010) observed by means of a lidar an increase of stratospheric aerosol loading over Spitsbergen after the minor eruption of the Kasatochi volcano in August 2008. The stratospheric aerosol enhancement above Halifax caused by the same eruption was observed by Bitar et al. (2010). Schmale et al. (2010)

Nabro volcano aerosol in the stratosphere from twilight spectrometry

N. Mateshvili et al.

Title Page

Abstract

Introduction

Conclusions

References

Tables

Figures

⏪

⏩

◀

▶

Back

Close

Full Screen / Esc

Printer-friendly Version

Interactive Discussion



Nabro volcano aerosol in the stratosphere from twilight spectrometry

N. Mateshvili et al.

Title Page

Abstract

Introduction

Conclusions

References

Tables

Figures

⏪

⏩

◀

▶

Back

Close

Full Screen / Esc

Printer-friendly Version

Interactive Discussion



below the horizon. This effect is especially strong after major volcanic eruptions when the aerosol load in the stratosphere increases dramatically. Photometric measurements of the twilight sky brightness at one or more wavelengths allow the retrieval of quantitative estimates of the stratospheric aerosol loading (e.g., Volz, 1975; Volz and Goody, 1962; Shakh, 1969; Mateshvili et al., 1998, 2005; Mateshvili and Rietmeijer, 2002). During a previous work (Mateshvili et al., 2005) stratospheric aerosol extinctions after the Pinatubo eruption in 1991 were retrieved from twilight measurements by using SDISORT (Dahlback and Stamnes, 1991), a pseudospherical radiative transfer code, that is part of the package Libradtran (<http://www.libradtran.org>).

In this paper we present lower stratospheric and upper tropospheric aerosol extinction profiles retrieved from ground-based spectral measurements of twilight sky brightness. The measurement dataset covers the period from October 2009 to August 2011. Radiative transfer computations in a Monte Carlo approach are used to feed the retrieval algorithm and to better understand the role of single and multiple scattering in the twilight period. We also consider measurements acquired in 1991, after the Pinatubo eruption, to analyze the phenomenon of the “second purple light”, the late reddening of twilight sky that is sometimes visible after the “first purple light”, when the Sun sinks deeper behind the horizon (Mateshvili et al., 2005).

2 The twilight sounding method

The twilight sounding method had been described in detail in (Mateshvili et al., 2005). Here we will briefly summarize the main ideas (Fig. 1).

During twilight when the solar zenith angle (SZA) is greater than 90° , the lower part of the atmosphere above the observer is shadowed and the upper part is sunlit. The boundary between shadowed and sunlit parts of the atmosphere shifts with the progress of twilight leaving the lower layers of the atmosphere in the Earth’s shadow. This gives us a natural possibility of atmospheric sounding.

When the Sun is below the horizon only the scattered light can be measured by a spectrometer. The intensity of the scattered light depends on the vertical extinction profiles of the different atmospheric species, as well as on aerosol and molecular phase functions.

3 Equipment

The measurements were carried out with two different instruments. The first is a CCD camera with a grating spectrograph which is operating nowadays while the second is a photometer that was used in the period 1990–1993. To distinguish between both datasets we will mark them as “dataset I” and “dataset II”.

3.1 Dataset I

The measurements were carried out in the period from October 2009 to August 2011 in Tbilisi, Georgia (41° 43′ N, 44° 47′ E). We used a SBIG ST-9XE CCD camera equipped with SBIG SGS spectrograph and a sunshade that allowed to reduce the field of view down to 4°. The spectrograph was adjusted to take spectra between 700 and 800 nm (see Sect. 5 for measurements wavelength discussion). The spectral resolution was 3.8 nm. The ST-9XE camera uses the KAF-0261E CCD from Kodak with 512 × 512 pixels and full well capacity (i.e. the amount of charge an individual pixel can hold before saturating) of $\sim 150\,000 e^-$ connected to a 16 bits A/D converter.

3.2 Dataset II

The measurements were carried out in November 1991, Abastumani, Georgia (41° 46′ N, 42° 50′ E), in rural conditions. A multi-channel photometer was equipped with interference filters (half-width $\Delta\lambda \approx 5$ nm) centered at $\lambda = 422, 474, 496, 542, 610, 642, 678, 713$ and 820 nm. The field of view of the optical channels corresponded to an angular diameter equal to 1°. More details can be found in (Mateshvili et al., 2005).

Nabro volcano aerosol in the stratosphere from twilight spectrometry

N. Mateshvili et al.

Title Page

Abstract

Introduction

Conclusions

References

Tables

Figures

⏪

⏩

◀

▶

Back

Close

Full Screen / Esc

Printer-friendly Version

Interactive Discussion



4 Measurements

4.1 Dataset I

Figure 2 shows an example of an acquired spectral image of the twilight sky. Pixels from the central part of the frame were averaged between the two red lines, corresponding to a spatial average, to get a twilight spectrum (Fig. 3a).

A wavelength calibration was achieved by attributing the observed atmospheric absorption water and oxygen bands (Fig. 3a) to the modeled ones (Fig. 3b). The pixel numbers were in this way converted to wavelengths.

The dark current was measured before every spectrum acquisition. The dark frames were subtracted from the measurement frames. Every spectrum was averaged (red rectangle area on Fig. 2) in the wavelength interval [775.5–782.5 nm]. Hereafter the dependence of the monochromatic intensity on SZA is called “twilight curve”. The choice of the wavelength will be discussed in Sect. 5.1.

The measurements were carried out in a SZA range of 88–100°. Figure 4 shows an example of measured light intensity in arbitrary units presented on a logarithmic scale. The viewing zenith angle (VZA) and azimuth were constant during an observation. The choice of the VZA and azimuth determine the angle at which light scatters on aerosol and air molecules towards the observer. Atmospheric aerosol particles are significantly larger than air molecules which lead to strong forward scattering. Light scattered towards the observer during a twilight event contains two components scattered respectively by aerosols and air molecules. Smaller scattering angles contain a larger aerosol component of the scattered light (Mateshvili et al., 2005, Fig. 5). This means that large VZAs and the boresight azimuth close to the solar direction create favorable conditions for aerosol detection. The VZA was chosen between 45–60°. This choice depended on the season and was imposed by the local topography. As the scattering angle is important it is necessary to know exactly the observational azimuth related to the solar one. To determine the viewing azimuth the spectrometer was pointed to the Sun just before a sunset. At that moment the viewing azimuth was

Nabro volcano aerosol in the stratosphere from twilight spectrometry

N. Mateshvili et al.

Title Page

Abstract

Introduction

Conclusions

References

Tables

Figures



Back

Close

Full Screen / Esc

Printer-friendly Version

Interactive Discussion



Nabro volcano aerosol in the stratosphere from twilight spectrometry

N. Mateshvili et al.

Title Page

Abstract

Introduction

Conclusions

References

Tables

Figures

⏪

⏩

◀

▶

Back

Close

Full Screen / Esc

Printer-friendly Version

Interactive Discussion

equal to the solar azimuth. The relative azimuth angle between the viewing direction and the following solar directions can be calculated from each spectrum acquisition time. Both solar azimuth and SZAs were calculated using the SPICE NAIF program package (<http://naif.jpl.nasa.gov/naif/toolkit.html>). Refraction effects are discussed in Sect. 5.3.2.

Twilight sky brightness decreases $\sim 10^5$ times in the SZA range from 88 to 100°. This exceeds the CCD dynamic range. Therefore each twilight observation consists of a few ensembles of measurements acquired with different exposure times. The ensembles are clearly visible in Fig. 4, they are separated by SZA gaps which correspond to time gaps necessary to change the exposure time. Usually three exposure times, 0.3, 2 and 20 s were used.

The measurements performed with different exposure times were reconnected by dividing by the corresponding exposure times. The sensitivity of the spectrometer and CCD detector has not been calibrated in an absolute way (see Sect. 5.1 for discussion). Hence, all measured intensities are in arbitrary units.

4.2 The Nabro eruption

The Dataset I cover the period after the minor eruption of the Nabro volcano. The eruption from Nabro (13° 22′ 12″ N, 41° 42′ 0″ E), a stratovolcano located in Eritrea started between 0 and 2 a.m. UT on 13 June 2011. An eruption plume initially rose to altitudes in between 9.1 and 13.7 km (Smithsonian institution, <http://www.volcano.si.edu/world/volcano.cfm?vnum=0201-101> \&volpage=weekly)

Fromm et al. (2013) analysed MODIS (Moderate Resolution Imaging Spectroradiometer) measurements and showed that at 2 h after the eruption volcanic plume was above the tropopause. Vernier et al. (2013) used CALIPSO (Cloud Aerosol Lidar and Infrared Pathfinder Satellite Observation) data to estimate the SO₂ cloud altitude. Two days after the eruption, the CALIPSO lidar crossed the main part of the volcanic SO₂ cloud. The volcanic cloud was detected near 15 to 17 km altitude, between 42° and 43.5° N.

Nabro volcano aerosol in the stratosphere from twilight spectrometry

N. Mateshvili et al.

Title Page

Abstract

Introduction

Conclusions

References

Tables

Figures



Back

Close

Full Screen / Esc

Printer-friendly Version

Interactive Discussion



Air parcel trajectories modeled by the web-based code Hysplit (<http://ready.arl.noaa.gov/HYSPLIT.php>) show that the air masses which have been above the volcano during the eruption at the plume altitude were transported towards Georgia (Fig. 5). Vernier et al. (2013) present a map of SO₂ index obtained from nighttime hyperspectral AIRS (Atmospheric InfraRed Sounder) data on 15 June 2011. The SO₂ enhancement above Georgia is clearly visible on the map.

Figure 6 shows two twilight curves. One was acquired on 24 June 2011 and has an unperturbed shape that is typical for the SAL background condition. Another was acquired on 14 July 2011 and was already perturbed by volcanic aerosols. The enhanced SAL manifests itself as a hump between 92° and 94° SZAs.

4.3 Dataset II

The measurements were carried out in the SZA range 89–107°. VZA was constant during an observation. Here we consider only measurements with a VZA of 60°. The viewing direction was kept in the solar azimuth by a computer-controlled alt-azimuthal mounting. Photomultipliers working in photon-counting mode were used as light receivers. The channel considered in this study was equipped with a filter centered at a wavelength of 713 nm.

The upper SZA limit is different for the two sets of measurements (100° for dataset I and 107° for dataset II). The lower value used for dataset I was imposed by the increase of the CCD exposure time necessary to measure the rapidly decreasing light intensity and by the level of light pollution in urban conditions. Dataset II was acquired in rural conditions and the upper limit of SZA represents the end of the twilight when the sky brightness is determined by the stellar background.

4.4 The Pinatubo eruption

The dataset II were acquired after the Pinatubo eruption, (Philippines, June 1991). We consider observations in November 1991, when the stratospheric aerosol layer was enhanced after the eruption.

5 The retrieval algorithm

5.1 The measurement vector

The twilight sky brightness was analyzed at 780 nm (dataset I). There is no gaseous absorption at this wavelength (except in the weak Wulf ozone band, see Sect. 6.6 for discussion) and therefore only the aerosol and molecular extinctions have to be considered. The molecular extinction can be calculated from the US standard atmosphere (see Sect. 6.6 for the atmospheric model choice discussion). The molecular extinction is weak at 780 nm, so the impact of the uncertainties due to deviations of the real atmospheric pressure and temperature profile from the climatological values is negligible. Hence, the aerosol extinction profile was the only profile to be retrieved.

The measurements were processed in the following way before applying the retrieval procedure. First, the twilight curves (monochromatic intensities versus SZA) were built. Since the light intensity changes by several orders of magnitude during twilight, it is easier to operate with the logarithm of the light intensity. To amplify the dynamics of the twilight curve and to remove all constant calibration factors, the measurement vector y was presented as the derivative of the logarithm of the twilight curve as a function of SZA:

$$y_i = \log \left(\frac{I_{i+1}}{I_i} \right) \quad (1)$$

Nabro volcano aerosol in the stratosphere from twilight spectrometry

N. Mateshvili et al.

Title Page

Abstract

Introduction

Conclusions

References

Tables

Figures

⏪

⏩

◀

▶

Back

Close

Full Screen / Esc

Printer-friendly Version

Interactive Discussion



where I is the measured light intensity. The SZA step ΔSZA was 0.1° . We do not divide this expression by ΔSZA because we consider ΔSZA as a constant factor with negligible uncertainty. Thus Eq. (1) is not a real derivative although we use this term.

5.2 The aerosol phase function

5 The aerosol phase function was approximated by the Heyney–Greenstein phase function, which is characterized by a single scattering albedo and an asymmetry factor. The single scattering albedo A_s and the asymmetry factor g_s for stratospheric sulfate aerosols can be estimated for volcanically quiet and volcanically disturbed conditions using the Mie theory and aerosol size distributions from the ECSTRA model (Fussen and Bingen, 1999). The aerosol complex refractive coefficient can be estimated using
10 the code developed by Krieger et al. (2000) and the temperature value taken from the US Standard Atmosphere. The estimates for volcanically quiet and volcanically perturbed stratospheric aerosols are $A_s = 1$ and $g_s = 0.65 \dots 0.75$.

The tropospheric aerosol single scattering albedo A_t and asymmetry factor g_t
15 were adopted from the Ankara AERONET site, which is closest to Tbilisi (<http://aeronet.gsfc.nasa.gov>). The aerosol optical parameters typically vary in the ranges $A_t = 0.72 \dots 0.87$, $g_t = 0.62 \dots 0.66$. The average values $A_t = 0.8$ and $g_t = 0.65$ were used in the retrieval procedure.

5.3 The forward model

20 5.3.1 The multiple scattering corrections

The sphericity of the atmosphere needs to be taken into account for the correct modeling of the twilight event. The best tool to model a 3-D spherical atmosphere at any SZA is a Monte Carlo simulation of the photon path. But a Monte Carlo code is too slow to be directly applied as a forward model for any retrieval procedure. To bypass this

Nabro volcano aerosol in the stratosphere from twilight spectrometry

N. Mateshvili et al.

Title Page

Abstract

Introduction

Conclusions

References

Tables

Figures

◀

▶

◀

▶

Back

Close

Full Screen / Esc

Printer-friendly Version

Interactive Discussion

problem a single scattering forward model with multiple scattering corrections obtained from the Monte Carlo code was developed.

For this purpose a reference aerosol extinction profile typical for volcanically quiet conditions was constructed from SAGE II (Stratospheric Aerosol and Gas Experiment) aerosol profiles. The Monte Carlo code Siro (Oikarinen et al., 1999) was used to model a twilight curve at 780 nm with the reference aerosol extinction profile as an input. The used number of photons was 10^6 , a trade off between acceptable computing time and the precision of the modeled curve. The calculations were repeated 10 times to obtain a standard deviation. This simulation allowed to estimate the fraction of the twilight intensity caused by single scattering and by multiple scattering. Figure 7a shows the modeled averaged ratio between the multiple and single scattering as a function of SZA for two aerosol profiles (Fig. 7b). Dashed lines show the Monte Carlo modeling standard deviations. Figure 7a shows that single scattering plays a dominant role in the SZA range 88–94°. However, the relative multiple scattering contribution depends on the aerosol loading. This contribution may be important (Fig. 7a, case 2). This means that the twilight light intensity cannot be presented as the single scattering with the multiple scattering correction because the multiple scattering is not a small constant factor for the SZA range of interest.

Let us consider the derivative of the logarithm of the intensity instead of the absolute values of twilight light intensity (Eq. 1). Figure 8 shows the modeled single scattering light intensity logarithmic derivatives (SS) together with the corresponding multiple scattering corrections (MS) for the logarithmic derivatives for the two different aerosol profiles considered in Fig. 7b. Let us compare the multiple scattering corrections presented in Fig. 7a and the corresponding logarithmic derivatives presented in Fig. 8. The multiple scattering correction curve for the logarithmic derivatives (Fig. 8) is almost zero at SZA < 93° and less sensitive to the aerosol profile at SZAs > 93°. It can be considered as a small correction with respect to the single scattering curve (Fig. 8). We can conclude that a single scattering approximation with multiple scattering corrections is sufficient when the modeled quantity is the logarithmic derivative of intensity.

Nabro volcano aerosol in the stratosphere from twilight spectrometry

N. Mateshvili et al.

Title Page

Abstract

Introduction

Conclusions

References

Tables

Figures

⏪

⏩

◀

▶

Back

Close

Full Screen / Esc

Printer-friendly Version

Interactive Discussion



Nabro volcano aerosol in the stratosphere from twilight spectrometry

N. Mateshvili et al.

Title Page

Abstract

Introduction

Conclusions

References

Tables

Figures

⏪

⏩

◀

▶

Back

Close

Full Screen / Esc

Printer-friendly Version

Interactive Discussion



5.3.2 The atmospheric refraction during a twilight event

The atmospheric refraction should be considered when modeling twilight sky brightness. The refraction mainly affects the long grazing direct sunrays before they undergo a single scattering towards the observer. Here the refraction effects were considered only in case of single scattering where they are more important. Refracted ray paths were modeled for different tangent altitudes and different SZAs as described in (Auer and Standish, 2000). Look-up tables of the refracted rays for every SZA were calculated and used in the forward model.

5.3.3 The angular size of the Sun

The Sun was considered as a disk with angular size $a = 32'$ that was divided into 20 horizontal strips. The center of the Sun corresponds to the actual SZA whereas the upper and lower points – to the SZA $\pm a/2$. Modeled twilight curves were integrated with SZA over the solar disk. The main consequence of the integration is twilight curve smoothing.

5.3.4 The instrument's field of view

Normally, the simulated twilight sky light intensities should be convolved with the instrument vertical field-of-view. Modeling shows that this convolution can be neglected in case if the measurement vector is presented as (Eq. 1).

6 The retrieval procedure

An error-weighted least-squares fitting to retrieve the aerosol extinction profiles was performed by means of a Levenberg–Marquardt algorithm.

The cost function was presented as:

$$\chi^2 = [\mathbf{y} - f(\mathbf{x})]^T \mathbf{S}_\varepsilon^{-1} [\mathbf{y} - f(\mathbf{x})] + (\mathbf{x} - \mathbf{x}_a)^T \mathbf{S}_a^{-1} (\mathbf{x} - \mathbf{x}_a) \quad (2)$$

4413

where the function $f(\mathbf{x})$ represents the forward model, \mathbf{x}_a is the a priori state vector, \mathbf{S}_a is the a priori covariance matrix, \mathbf{S}_ϵ is the measurement error covariance matrix and \mathbf{y} is the measurement vector (Eq. 1).

The a priori state vector with its uncertainties σ_a is presented in Fig. 9. The a priori covariance matrix was constructed as follows:

$$\mathbf{S}_a^{i,j} = \sigma_a^i \sigma_a^j \exp\left(-|i-j| \frac{\delta z}{h}\right) \quad (3)$$

where $\sigma_a^{i,j}$ are uncertainties presented in Fig. 9, $\delta z = 1$ km is the difference between two altitude levels and $h = 3$ is a scale parameter that controls the altitude correlation length.

To construct the measurement error covariance matrix both uncertainties of the measurements and uncertainties of the forward model should be considered.

6.1 Measurements errors

CCD noise can be estimated using formulas from (Merline and Howell, 1995).

The signal averaged over a spectral image wavelength dimension and space dimension (Fig. 2, red square) is known within a standard deviation with respect to the derived mean value. This error is included in the retrieval algorithm. Other measurement errors are systematic errors (systematic for a particular twilight curve) such as the SZA error, which arise from the time error, VZA error and azimuth error. The VZA error arises from pointing uncertainty and from the extension of the field of view. The azimuth error arises from pointing uncertainty and time uncertainty.

The modeling shows that the systematic errors mentioned above can be neglected if the measurement vector is presented as (Eq. 1).

Nabro volcano aerosol in the stratosphere from twilight spectrometry

N. Mateshvili et al.

Title Page

Abstract

Introduction

Conclusions

References

Tables

Figures

⏪

⏩

◀

▶

Back

Close

Full Screen / Esc

Printer-friendly Version

Interactive Discussion

6.2 Forward model errors

The most important uncertainty comes from the forward model. It has three components: the random error from the Monte Carlo simulation, the systematic error introduced by the forward model simplifications described in Sect. 5 and systematic errors induced by the atmospheric model and climatological values of single scattering albedo and asymmetry factor.

6.3 The random error from the Monte Carlo simulation

To estimate the Monte Carlo error, the associated computations have been repeated 10 times with the same aerosol extinction profile. The number of photons was 10^6 . The error was calculated as a standard mean square deviation. It makes no sense to increase the number of photons to achieve a smaller value of uncertainty, because the expected natural aerosol profile variability will cause variations of multiple scattering correction larger than the Monte Carlo simulation uncertainties.

6.4 Forward model simplification error

The main simplification in the forward model is the assumption that a single scattering radiative transfer code with multiple scattering corrections calculated using a fully spherical Monte Carlo code, combined with an a priori aerosol profile, can be used instead of a fully spherical radiative transfer code. Multiple scattering error increases with SZA (Fig. 8). Therefore it is important to know the SZA upper limit below which such simplification can be applied.

Aerosol extinction profiles were retrieved from a few twilight measurements acquired before and after the Nabro volcano eruption. The retrieved aerosol profiles were used as an input in the Monte Carlo code to estimate the real multiple scattering corrections. The real and a priori multiple scattering corrections coincide within the limits of

Nabro volcano aerosol in the stratosphere from twilight spectrometry

N. Mateshvili et al.

Title Page

Abstract

Introduction

Conclusions

References

Tables

Figures

⏪

⏩

◀

▶

Back

Close

Full Screen / Esc

Printer-friendly Version

Interactive Discussion



uncertainty below $\text{SZA} \approx 94^\circ$ for the background aerosol case and below $\text{SZA} \approx 93.5^\circ$ after the eruption. Therefore these SZA upper limits will be used for the retrieval.

6.5 Clouds and hazes near the observer and near the terminator

In this section we investigate if local hazes, fogs and local and remote clouds influence the measured twilight sky brightness. We should mention that all twilight observations were carried out in visibly clear sky conditions. Twilight measurements from $\text{SZA} = 90^\circ$ to $\text{SZA} = 94^\circ$ take about 24 min and therefore the bottom layer aerosol optical depth can be assumed relatively stable.

The modeling was performed using the fully spherical single scattering model with multiple scattering corrections described above. The derivatives of the logarithm of the modeled light intensity were calculated (see Eq. 1).

The following scenarios were considered: an aerosol layer near the surface above the observer's position and clouds at different altitudes and at different distances from the observer (see Mateshvili et al., 2012 for details). We have concluded that a stable aerosol layer near the observer and remote clouds do not disturb the measurement vector. The former contributes only in absorption and decreases the modeled light intensities by a constant factor. This factor is removed by taking the derivative of logarithm of intensity. Since the lower layers of the atmosphere are almost opaque for slant solar rays due to Rayleigh scattering and some background tropospheric aerosol, the presence of remote clouds does not change the modeled twilight sky intensities. Only close clouds disturb the modeled intensities, but they should be within the field of vision which was not the case.

6.6 Forward model parameters errors

These errors are not included in the retrieval algorithm.

In the forward model we made use of the US standard atmosphere. The error due to the deviations of the real atmospheric parameters from the standard ones was

Nabro volcano aerosol in the stratosphere from twilight spectrometry

N. Mateshvili et al.

Title Page

Abstract

Introduction

Conclusions

References

Tables

Figures

◀

▶

◀

▶

Back

Close

Full Screen / Esc

Printer-friendly Version

Interactive Discussion



Nabro volcano aerosol in the stratosphere from twilight spectrometry

N. Mateshvili et al.

Title Page

Abstract

Introduction

Conclusions

References

Tables

Figures

◀

▶

◀

▶

Back

Close

Full Screen / Esc

Printer-friendly Version

Interactive Discussion



estimated by comparing the retrieved aerosol profiles for three cases: (1) the standard atmosphere, (2) midlatitude summer atmosphere and (3) midlatitude winter atmosphere. The differences between the three retrieved aerosol profiles are well within the standard deviation of the retrieval.

To estimate the errors caused by deviations of the asymmetry factor and the single scattering albedo from the climatological values (see Sect. 5.2) the aerosol extinction profiles were retrieved from the same observations using the extreme values of the optical parameters. The estimated uncertainties appeared to be strongly dependent on the particular aerosol extinction profiles. Therefore the uncertainties were calculated for the averaged stratospheric optical depths (see Sect. 6.9, Eq. 9). Stratospheric aerosol asymmetry factors $g_s = 0.65$; 0.7; 0.75, tropospheric aerosol single scattering albedos $A_t = 0.72$; 0.8; 0.87 and tropospheric aerosol asymmetry factors $g_t = 0.62$; 0.65 were used. The corresponding uncertainties were: 4%–27%, 4%–10%, 1%–13%.

We can conclude that the systematic uncertainties caused by aerosol optical parameters uncertainties vary significantly and should be estimated for the particular dataset.

The neglected ozone absorption by weak ozone Wulf band (http://igaco-o3.fmi.fi/ACSO/cross_sections.html) creates a radiance error of about 2% at SZA = 88° and 8% at SZA = 95°. But the logarithmic derivative practically does not change.

6.7 Logarithmic derivative uncertainties

All uncertainties discussed above are uncertainties on the intensity whereas in the retrieval algorithm the logarithmic derivative of the intensity is used as a forward model. This means that the uncertainties should be modified before to be included in the retrieval algorithm. The transformed signal is:

$$F = \log(I_{i+1}/I_i) \quad (4)$$

where I_i are discretized light intensities. In this case the mean squared standard deviation σ is:

$$\sigma(F)^2 = \sigma(I_{i+1})^2/I_{i+1}^2 + \sigma(I_i)^2/I_i^2 \quad (5)$$

6.8 The retrieved aerosol extinction profile uncertainties and averaging kernels

The retrieved aerosol extinction profile uncertainties were estimated from the retrieval Jacobian. The retrieval covariance matrix \mathbf{S} is connected with the Jacobian \mathbf{K} as follows (Rodgers, 2000):

$$5 \quad \mathbf{S}^{-1} = \mathbf{K}^T \mathbf{S}_\varepsilon^{-1} \mathbf{K} + \mathbf{S}_a^{-1} \quad (6)$$

The diagonal elements of the covariance matrix represent the squares of the uncertainties for the corresponding extinction values.

The averaging kernel matrix is given by:

$$\mathbf{A} = \left(\mathbf{K}^T \mathbf{S}_\varepsilon^{-1} \mathbf{K} + \mathbf{S}_a^{-1} \right) \mathbf{K}^T \mathbf{S}_\varepsilon^{-1} \mathbf{K} \quad (7)$$

10 The rows of \mathbf{A} show the resolution of the retrieved profile, the columns give the response of the system to a delta function in the corresponding altitude.

The number of degrees of freedom for signal d_s was estimated as a sum of the diagonal elements of \mathbf{A} .

6.9 Stratospheric optical depth's uncertainties

15 The variance of the individual observation stratospheric optical depth was estimated as

$$\sigma_\tau^2 = \sum_i^n \sum_j^n S_{ij} \quad (8)$$

where S_{ij} are the retrieval covariance matrix elements and n is the number of altitude points.

Nabro volcano aerosol in the stratosphere from twilight spectrometry

N. Mateshvili et al.

Title Page

Abstract

Introduction

Conclusions

References

Tables

Figures

◀

▶

◀

▶

Back

Close

Full Screen / Esc

Printer-friendly Version

Interactive Discussion

The weighted average optical depth over a set of observations:

$$\tau_{\text{av}} = \frac{\sum_i^N \varpi_i \tau_i}{\sum_i^N \varpi_i}, \quad \varpi_i = \sigma_i^{-2} \quad (9)$$

where τ_i are stratospheric optical depths with variances σ_i calculated from individual observations, N – number of observations in the set.

The variance of the average is:

$$\sigma_{\text{av}}^2 = \left(\sum_i^N \varpi_i \right)^{-1} \quad (10)$$

7 Results and discussion

7.1 Aerosol extinction profiles – Dataset I

Figures 10–12 present three typical examples of measured twilight curves fitted by the modeled ones (a), the retrieved aerosol extinction profiles (b) and corresponding averaging kernels (c, d). The experimental and the modeled twilight curves have been shifted to coincide at $\text{SZA} = 92^\circ$. This is necessary because in the retrieval algorithm it is not the twilight curves but their logarithmic derivatives that are used. Figure 10 corresponds to the background aerosol loading, Figs. 11 and 12 to the volcanically disturbed aerosol layer observed after the Nabro eruption.

For background stratospheric aerosol loading conditions the uncertainties of the retrieved aerosol extinction are high (Fig. 10b). The averaging kernel matrix (Fig. 10c) shows that the vertical resolution was about 2 km in the upper troposphere and about 6 km in the stratosphere (Fig. 10d).

Nabro volcano aerosol in the stratosphere from twilight spectrometry

N. Mateshvili et al.

Title Page

Abstract

Introduction

Conclusions

References

Tables

Figures

⏪

⏩

◀

▶

Back

Close

Full Screen / Esc

Printer-friendly Version

Interactive Discussion

Uncertainties decrease at the layer altitude for the enhanced stratospheric aerosol layer after the Nabro eruption (Figs. 11–12b), which simply means that aerosol influences the signal more strongly. The averaging kernel matrix (Fig. 11–12c, d) show that the vertical resolution is very nonuniform and increases up to 1.5–2 km just below the layer. Aerosol extinctions below 5 km are strongly affected by the upper layers and are not reliable.

To investigate the retrieved aerosol profiles variability for each altitude the 15.87 %, 50 % and 84.13 % percentiles were calculated from an ensemble of retrievals. The 50 % percentile is the median value, the 15.87 % and 84.13 % percentiles represent the distribution width. Dataset I was divided in four parts: fall 2009–winter 2010 (Fig. 13a), spring–summer 2010 (Fig. 13b), fall 2010–winter 2011 (Fig. 13c) and summer 2011 (Fig. 13d). Figure 13a–c correspond to the background stratospheric aerosol conditions, Fig. 13d – volcanically disturbed after the Nabro eruption. The volcanic stratospheric aerosol layer persisted at about 17 km altitude during the end of July–beginning of August 2011.

The enhanced stratospheric aerosol layer was observed just above the tropopause. The tropopause altitude for Tbilisi in July 2011 was 16 km. It was derived from the real temperature and pressure profile extracted from ECMWF data (The European Centre for Medium-Range Weather Forecast, <http://www.ecmwf.int/products/data/archive/>).

To estimate stratospheric aerosol loading all retrieved aerosol profiles were integrated above 16 km. The optical depths are $6.1 \times 10^{-3} \pm 2.1 \times 10^{-3}$ (31 August 2009–29 November 2009, 15 observations), $2.3 \times 10^{-3} \pm 7.6 \times 10^{-4}$ (20 March 2010–30 August 2010, 27 obs.), $3.0 \times 10^{-3} \pm 1.2 \times 10^{-3}$ (01 September 2010–15 January 2011, 23 obs.), and $1.1 \times 10^{-2} \pm 2.6 \times 10^{-3}$ (18 July 2011–03 August 2011, 10 obs.). The uncertainties were calculated as was described in Sect. 6.9. Although the tropopause altitude is lower than 16 km in winter the same low limit of integration over altitude was taken for all observations to make the result comparable. The stratospheric aerosol loading was 2–3 times higher after the eruption than in background conditions.

Nabro volcano aerosol in the stratosphere from twilight spectrometry

N. Mateshvili et al.

Title Page

Abstract

Introduction

Conclusions

References

Tables

Figures

◀

▶

◀

▶

Back

Close

Full Screen / Esc

Printer-friendly Version

Interactive Discussion



The Nabro aerosol layer was observed at 17–18 km by lidar over Japan (Uchino et al., 2012). CALIPSO measurements over both North Africa and the monsoon region on 1 July show extended aerosol layers at altitudes up to 20 km (Bourassa et al., 2012). The data on the layer altitude are in good agreement with our results.

Bourassa et al. (2012) showed the weekly zonal mean stratospheric aerosol optical depth at 750 nm estimated from OSIRIS (Optical Spectrograph and Infra-Red Imaging System) measurements. The stratospheric aerosol optical depth in the regions affected by Nabro eruption varied in range $8\text{--}12 \times 10^{-3}$ which is very close to our result. Their background aerosol level ($2\text{--}4 \times 10^{-3}$) also reasonably agrees with our estimates. The relatively elevated level (6.1×10^{-3}) of the background stratospheric aerosol optical depth estimated within the period 31 August 2009–29 November 2009 is caused by the Sarychev Peak (48°N , 153°E) eruption in the middle of June 2009 (Mattis et al., 2010, http://www.nasa.gov/multimedia/imagegallery/image_feature_1397.html).

7.2 Twilight sky brightnesses at SZAs larger than 95°

As we have seen above stratospheric aerosol disturbs significantly twilight sky brightness in the SZA range $91\text{--}95^\circ$. It is interesting to see if the presence of volcanic aerosol can disturb twilight sky brightness at higher SZAs.

The Dataset I was acquired in city conditions and therefore the measurements at SZAs larger than 95° were strongly affected by light pollution. To understand how stratospheric aerosols can affect twilight sky brightness at higher SZAs we consider the Dataset II – the measurements, acquired in rural conditions. To model twilight sky brightnesses at high SZAs the Monte Carlo technique was used.

7.3 The second purple light, Dataset II

The phenomenon of the second purple light observed after the Pinatubo eruption was discussed in (Mateshvili et al., 2005). More specifically this phenomenon consists of a twilight sky brightness enhancement at large SZAs of $97\text{--}102^\circ$ (Fig. 14a, red dashed

Nabro volcano aerosol in the stratosphere from twilight spectrometry

N. Mateshvili et al.

Title Page

Abstract

Introduction

Conclusions

References

Tables

Figures

⏪

⏩

◀

▶

Back

Close

Full Screen / Esc

Printer-friendly Version

Interactive Discussion



line). This phenomenon is reported to be observed also after the Krakatoa eruption in 1889 (William Ascroft, contemporary English painter made a lot of sketches of spectacular twilights after the eruption, see <http://www.scienceandsociety.co.uk/results.asp?image=10316149&wwwflag={\&}imagepos=8{\&}screenwidth=1280>).

The associated aerosol extinction profile presented in Fig. 14b (black line) was retrieved from a twilight measurement acquired after the Pinatubo eruption in 1991. The SAGE II (Stratospheric Aerosol and Gas Experiment) extinction profiles interpolated spectrally to the wavelength of our measurements 713 nm are shown for comparison (green lines). The coincidence criteria between twilight and SAGE II observations were one day and 1000 km.

The Monte Carlo code Siro was used to model twilight sky intensities at high SZAs. Figure 14a shows two experimental (Dataset II) and two modeled twilight curves. The red and black dashed curves are measurements after and before the Pinatubo eruption. The red and blue solid curves were modeled. The blue solid curve was modeled using the retrieved aerosol profile (Fig. 14b, black curve). There is no second purple light signature on the modeled curve, it is very close to the twilight curve measured in the background conditions (black dashed). It is clearly necessary to derive conditions in which the second purple light will be visible. Therefore, a new aerosol profile was constructed (Fig. 14b, red line). The SAL was not changed but the aerosol extinction below it was decreased. In this case the second purple light becomes clearly visible (Fig. 14a, red solid curve). The first purple light also increased and does not coincide any more with the measurements (red dashed curve). This discrepancy between the modeling and measurements can be explained by a different transparency below the SAL in the vicinity of the observational place and at large distances. When the SAL is a few kilometers above the tropopause the aerosol extinction between the tropopause and the SAL can be low. In such conditions the scattered light passes under the SAL through the zone of low aerosol extinction and scatters again inside the SAL.

Figure 14c shows the contribution of single (red) and double (black) scattering to the second purple light modeled with Siro. It is clear that the second purple light is caused by multiple scattering in the stratospheric aerosol layer.

7.4 Mesospheric clouds

In the previous section we have considered how multiple scattering can increase the twilight sky brightness at large SZAs. It is interesting to see if single scattering on aerosol at high altitude can cause the same effect. The Monte Carlo code was used in order to determine a quantity of mesospheric aerosol necessary to disturb the twilight sky brightness. Figure 15a shows the twilight curve with (solid red) and without (solid black) mesospheric aerosol layer. Dashed lines are single scattering contributions, where the red color corresponds to the case with the layer and the black color – to the case without the layer. Lumpe et al. (2008) presented Southern Hemisphere polar mesospheric cloud observations from the POAM (Polar Ozone and Aerosol Measurement) instrument. Their results for cloud extinctions at 442 nm show extinction variations from 10^{-7} km^{-1} up to 10^{-4} km^{-1} . Above, we assumed cloud layer (dashed line) with an extinction of 10^{-5} km^{-1} at 80–85 km altitude (Fig. 15b, red line). The wavelength of modeling was 440 nm. The atmospheric refraction effects were considered only for single scattering.

It is clear that the mesospheric layer with an extinction of 10^{-5} km^{-1} creates an additional sky brightness that is strong enough to be detected. This result is of course to be expected because the noctilucent clouds can be observed from the Earth's surface by naked eye in deep twilight.

Polar mesospheric clouds are composed of particles with effective radii of tens of nanometers (e.g., Lumpe et al., 2008). For such small particles the extinction decreases quickly with the wavelength. The extinction of the mesospheric aerosol layer presented in Fig. 15b is about 10 times lower at 780 nm, the wavelength of our measurements, than at 440 nm. This makes the layer undetectable at 780 nm. Thus, the two phenomena – the “second purple light” and the single scattering by the mesospheric

Nabro volcano aerosol in the stratosphere from twilight spectrometry

N. Mateshvili et al.

Title Page

Abstract

Introduction

Conclusions

References

Tables

Figures

◀

▶

◀

▶

Back

Close

Full Screen / Esc

Printer-friendly Version

Interactive Discussion



the stratospheric aerosol optical depth in the regions affected by Nabro eruption as $8\text{--}12 \times 10^{-3}$, using OSIRIS measurements. These values are close to our estimates.

The averaging kernels show that the vertical resolution in the stratosphere depends also on aerosol loading. In background conditions stratospheric aerosol vertical resolution is about 6 km, and decreases to 2 km in presence of volcanic aerosol.

The detected Nabro SAL altitude was 17 km. The layer altitude is in good agreement with lidar measurements (Bourassa et al., 2012; Uchino et al., 2012).

A few months after the Pinatubo eruption in November 1991 a “second purple light” phenomenon was observed (Mateshvili et al., 2005). The retrieved aerosol profile was used to model the “second purple light”, an enhancement of twilight sky brightness at large SZAs of $97\text{--}102^\circ$, (Fig. 14). The modeling results show that the “second purple light” is caused by multiple scattering in the stratospheric aerosol layer. The necessary condition to observe the “second purple light” is a high transparency zone below the SAL.

An enhancement of the twilight sky brightness at large SZA can be caused not only by multiple scattering in the SAL but also by single scattering at high altitude. The presence of a noctilucent cloud was modeled by introducing an aerosol layer with an extinction of 10^{-5} km^{-1} at 80–85 km altitude. The Monte-Carlo modeling at a wavelength of 440 nm shows that such a layer can create a measurable increase of the twilight sky brightness (Fig. 15).

We conclude that the used technique based on twilight sky brightness measurements allow to separate stratospheric and tropospheric aerosol optical depths and estimate stratospheric aerosol loading with reasonable uncertainties. The retrieved aerosol extinction profiles for volcanically perturbed periods have acceptable uncertainties. The twilight sounding method is therefore a good complement to other ground-based methods.

Acknowledgements. We thank the Georgian National Scientific Foundation for the spectrometer purchase and support (GNSF/ST06/5-097).

Nabro volcano aerosol in the stratosphere from twilight spectrometry

N. Mateshvili et al.

Title Page

Abstract

Introduction

Conclusions

References

Tables

Figures



Back

Close

Full Screen / Esc

Printer-friendly Version

Interactive Discussion



References

- Auer, L. H. and Standish, E. M.: Astronomical refraction: computational method for all zenith angles, *Astron. J.*, 119, 2472–2474, 2000.
- Bauman, J. J., Russell, P. B., Geller, M. A., and Hamill, P.: A stratospheric aerosol climatology from SAGE II and CLAES measurements: 2. Results and comparisons, 1984–1999, *J. Geophys. Res.*, 108, D13, 4383, doi:10.1029/2002JD002993, 2003.
- Bitar, L., Duck, T. J., Kristiansen, N. I., Stohl, A., and Beauchamp, S.: Lidar observations of Kasatochi volcano aerosols in the troposphere and stratosphere, *J. Geophys. Res.*, 115, D2, D00L13, doi:10.1029/2009JD013650, 2010.
- Bourassa, A. E., Degenstein, D. A., Elash, B. J., and Llewellyn, E. J.: Evolution of the stratospheric aerosol enhancement following the eruptions of Okmok and Kasatochi: Odin- OSIRIS measurements, *J. Geophys. Res.*, 115, D2, D00L03, doi:10.1029/2009JD013274, 2010.
- Bourassa, A. E., Robock, A., Randel, W. J., Deshler, T., Rieger, L. A., Lloyd, N. D., Llewellyn, E. J., and Degenstein, D. A.: Large volcanic aerosol load in the stratosphere linked 15 to Asian monsoon transport, *Science*, 337, 78–81, doi:10.1126/science.1219371, 2012.
- Brock, C. A., Hamill, P., Wilson, J. C., Jonsson, H. H., and Chan, K. R.: Particle formation in the upper tropical troposphere: a source of nuclei for the stratospheric aerosol, *Science*, 270, 1650–1653, 1995.
- Dahlback, A. and Stamnes, K.: A new spherical model for computing the radiation field available for photolysis and heating at twilight, *Planet. Space Sci.*, 39, 671–683, 1991.
- Fromm, M., Nedoluha, G., and Charvát, Z.: Comment on “large volcanic aerosol load in the stratosphere linked to asian monsoon transport”, *Science*, 339, 647, doi:10.1126/science.1228605, 2013.
- Fussen, D. and Bingen, C.: A volcanism dependent model for the extinction profile of stratospheric aerosols in the UV-visible range, *Geophys. Res. Lett.*, 26, 703–706, 1999.
- Hendricks, J., Lippert, E., Petry, H., and Ebel, A.: Heterogeneous reactions on and in sulfate aerosols: implications for the chemistry of the midlatitude tropopause region, *J. Geophys. Res.*, 104, 5531–5550, doi:10.1029/1998JD100098, 1999.
- Hoffmann, A., Ritter, C., Stock, M., Maturilli, M., Eckhardt, S., Herber, A., and Neuber, R.: 30 Lidar measurements of the Kasatochi aerosol plume in August and September 2008 in Ny-Ålesund, Spitsbergen, *J. Geophys. Res.*, 115, D2, D00L12, doi:10.1029/2009JD013039, 2010.

Nabro volcano aerosol in the stratosphere from twilight spectrometry

N. Mateshvili et al.

Title Page

Abstract

Introduction

Conclusions

References

Tables

Figures

◀

▶

◀

▶

Back

Close

Full Screen / Esc

Printer-friendly Version

Interactive Discussion



Nabro volcano aerosol in the stratosphere from twilight spectrometry

N. Mateshvili et al.

Title Page

Abstract

Introduction

Conclusions

References

Tables

Figures

⏪

⏩

◀

▶

Back

Close

Full Screen / Esc

Printer-friendly Version

Interactive Discussion



- Hofmann, D., Barnes, J., O'Neill, M., Trudeau, M., and Neely, R.: Increase in background stratospheric aerosol observed with lidar at Mauna Loa Observatory and Boulder, Colorado, *Geophys. Res. Lett.*, 36, L15808, doi:10.1029/2009GL039008, 2009.
- Krieger, U. K., Mössinger, J. C., Luo, B., Weers, U., and Peter, T.: Measurement of the refractive indices of H_2SO_4 HNO_3 H_2O solutions to stratospheric temperatures, *Appl. Optics*, 39, 3691–3703, 2000.
- Lumpe, J. D., Alfred, J. M., Shettle, E. P., and Bevilacqua, R. M.: Ten years of Southern Hemisphere polar mesospheric cloud observations from the polar ozone and aerosol measurement instruments, *J. Geophys. Res.*, 113, D04205, doi:10.1029/2007JD009158, 2008.
- Mateshvili, N. and Rietmeijer, F. J. M.: Stratospheric dust loading from early 1981 to September 1985 based on the twilight sounding method and stratospheric dust collection, *J. Volcanol. Geotherm. Res.*, 120, 55–69, 2002.
- Mateshvili, I., Mateshvili, G., and Mateshvili, N.: Measurement of the vertical aerosol distribution in the middle atmosphere by the twilight sounding method, *J. Aerosol Sci.*, 29, 1189–1198, 1998.
- Mateshvili, N., Fussen, D., Vanhellemont, F., Bingen, C., Kyrölä, E., Mateshvili, I., and Mateshvili, G.: Twilight sky brightness measurements as a useful tool for stratospheric aerosol investigations, *J. Geophys. Res.*, 110, D09209, doi:10.1029/2004JD005512, 2005.
- Mateshvili, N., Fussen, D., Mateshvili, G., Mateshvili, I., Vanhellemont, F., Kyrölä, E., Tukiainen, J., Kujanpää, S., Bingen, C., Robert, C., Tétard, C., and Dekemper, E.: Remote sensing of stratospheric and upper tropospheric aerosols by means of ground-based twilight sky spectral photometry, *Proc. of "ATMOS 2012 – Advances in Atmospheric Science and Applications"*, Bruges, Belgium, ESA SP-708, November 2012, 2012.
- Mattis, I., Siefert, P., Müller, D., Tesche, M., Hiebsch, A., Kanitz, T., Schmidt, J., Finger, F., Wandinger, U., and Ansmann, A.: Volcanic aerosol layers observed with multiwavelength Raman lidar over central Europe in 2008–2009, *J. Geophys. Res.*, 115, D00L04, doi:10.1029/2009JD013472, 2010.
- Merline, W. J. and Howell, S. B.: A realistic model for point-sources imaged on array detectors: the model and initial results, *Exp. Astron.*, 6, 163–210, doi:10.1007/BF00421131, 1995.
- Oikarinen, L., Sihvola, E., and Kyrölä, E.: Multiple scattering radiance in limb-viewing geometry, *J. Geophys. Res.*, 104, 31261–31274, doi:10.1029/1999JD900969, 1999.

Nabro volcano aerosol in the stratosphere from twilight spectrometry

N. Mateshvili et al.

Title Page

Abstract

Introduction

Conclusions

References

Tables

Figures

◀

▶

◀

▶

Back

Close

Full Screen / Esc

Printer-friendly Version

Interactive Discussion

- Ramachandran, S., Ramaswamy, V., Stenchikov, G. L., and Robock, A.: Radiative impact of the Mount Pinatubo volcanic eruption: lower stratospheric response, *J. Geophys. Res.*, 105, 24409–24430, doi:10.1029/2000JD900355, 2000.
- Rodgers, C. D.: Inverse methods for atmospheric sounding: theory and practice, in: *Atmospheric, Oceanic and Planetary Physics*, vol. 2, World Scientific, Singapore, 2000.
- Schmale, J., Schneider, J., Jurkat, T., Voigt, C., Kalesse, H., Rautenhaus, M., Lichtenstern, M., Schlager, H., Ancellet, G., Arnold, F., Gerding, M., Mattis, I., Wendisch, M., and Borrmann, S.: Aerosol layers from the 2008 eruptions of Mount Okmok and Mount Kasatochi: in situ upper troposphere and lower stratosphere measurements of sulfate and organics over Europe, *J. Geophys. Res.*, 115, D00L07, doi:10.1029/2009JD013628, 2010.
- Shakh, G. M.: Enhanced twilight glow caused by the volcanic eruption on Bali island in March and September 1963, *Tellus*, 21, 636–640, 1969.
- Solomon, S., Daniel, J. S., Neely, R. R., Vernier, J.-P., Dutton, E. G., and Thomason, L. W.: The persistently variable “background” stratospheric aerosol layer and global climate change, *15 Science*, 333, 866–70, doi:10.1126/science.1206027, 2011.
- Uchino, O., Sakai, T., Nagai, T., Nakamae, K., Morino, I., Arai, K., Okumura, H., Takubo, S., Kawasaki, T., Mano, Y., Matsunaga, T., and Yokota, T.: On recent (2008–2012) stratospheric aerosols observed by lidar over Japan, *Atmos. Chem. Phys.*, 12, 11975–11984, doi:10.5194/acp-12-11975-2012, 2012.
- Vanhellemont, F., Fussen, D., Mateshvili, N., Tétard, C., Bingen, C., Dekemper, E., Loodts, N., Kyrölä, E., Sofieva, V., Tamminen, J., Hauchecorne, A., Bertaux, J.-L., Dalaudier, F., Blanot, L., Fanton d’Andon, O., Barrot, G., Guirlet, M., Fehr, T., and Saavedra, L.: Optical extinction by upper tropospheric/stratospheric aerosols and clouds: GOMOS observations for the period 2002–2008, *Atmos. Chem. Phys.*, 10, 7997–8009, doi:10.5194/acp-10-7997-2010, 2010.
- Vernier, J.-P., Thomason, L. W., and Kar, J.: CALIPSO detection of an Asian tropopause aerosol layer, *Geophys. Res. Lett.*, 38, L07804, doi:10.1029/2010GL046614, 2011a.
- Vernier, J.-P., Thomason, L. W., Pommereau, J.-P., Bourassa, A., Pelon, J., Garnier, A., Hauchecorne, A., Blanot, L., Treppe, C., Degenstein, D., and Vargas, F.: Major influence of tropical volcanic eruptions on the stratospheric aerosol layer during the last decade, *Geophys. Res. Lett.*, 38, L12807, doi:10.1029/2011GL047563, 2011b.

Vernier, J.-P., Thomason, L. W., Fairlie, T. D., Minnis, P., Palikonda, R., and Bedka, K. M.: Comment on “large volcanic aerosol load in the stratosphere linked to asian monsoon transport”, *Science*, 339, 647, doi:10.1126/science.1227817, 2013.

Volz, F.: Volcanic twilights from Fuego eruption, *Science*, 189, 48–50, 1975.

- 5 Volz, F. and Goody, R.: The intensity of the twilight and upper atmospheric dust, *J. Atmos. Sci.*, 19, 385–406, 1962.

AMTD

6, 4401–4444, 2013

Nabro volcano aerosol in the stratosphere from twilight spectrometry

N. Mateshvili et al.

Title Page

Abstract

Introduction

Conclusions

References

Tables

Figures

⏪

⏩

◀

▶

Back

Close

Full Screen / Esc

Printer-friendly Version

Interactive Discussion



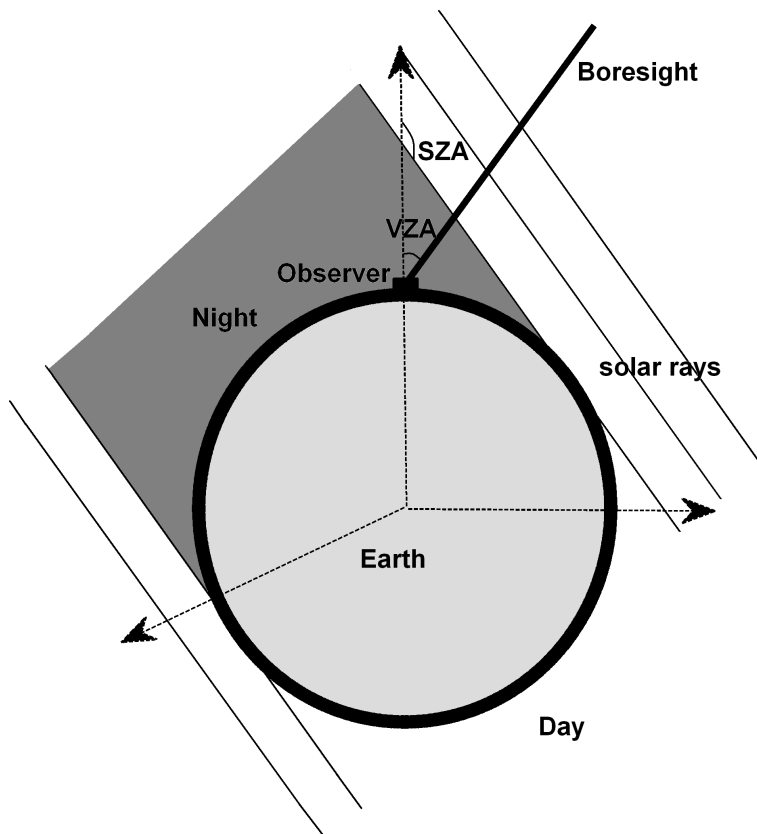


Fig. 1. The scheme of the twilight event. SZA is solar zenith angle, VZA – viewing zenith angle. Refraction is not shown in order to make the figure as simple as possible.

Nabro volcano aerosol in the stratosphere from twilight spectrometry

N. Mateshvili et al.

Title Page	
Abstract	Introduction
Conclusions	References
Tables	Figures
◀	▶
◀	▶
Back	Close
Full Screen / Esc	
Printer-friendly Version	
Interactive Discussion	



Nabro volcano aerosol in the stratosphere from twilight spectrometry

N. Mateshvili et al.

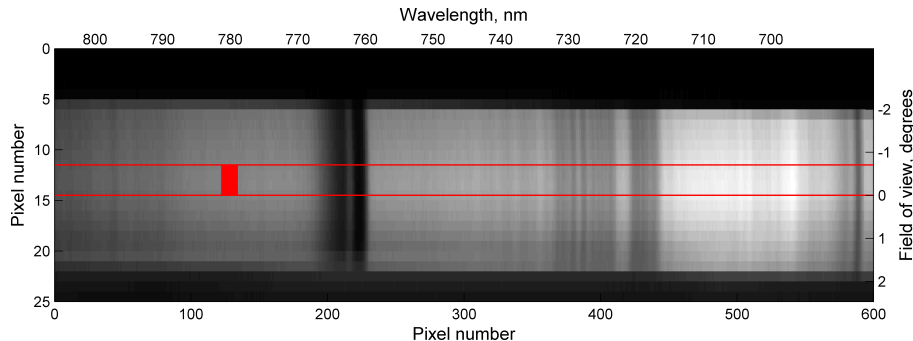


Fig. 2. The CCD image presents a twilight spectral image (685–800 nm) acquired by the spectrometer. Abscissa corresponds to wavelength dimension, ordinate – to spatial dimension. The spatial dimension is shown in degrees, because the distance to the scattering volume varies with the SZAs. Red lines encompass the spatial area where the spectral image was averaged. The red rectangle indicates the area where the spectral image was averaged to receive the monochromatic twilight sky intensity for the corresponding time.

Title Page

Abstract

Introduction

Conclusions

References

Tables

Figures

⏪

⏩

◀

▶

Back

Close

Full Screen / Esc

Printer-friendly Version

Interactive Discussion



Nabro volcano aerosol in the stratosphere from twilight spectrometry

N. Mateshvili et al.

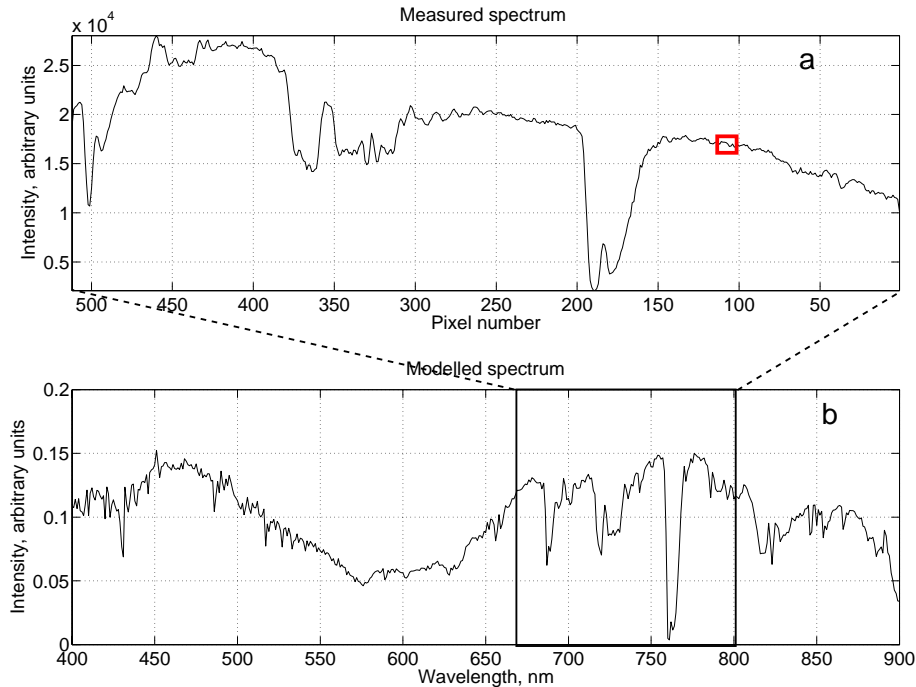


Fig. 3. An example of the measured (a) and the modeled (b) twilight spectrum. The red rectangle in panel (a) indicates the averaging area. The black square in panel (b) marks the same wavelength area as is presented in panel (a). Many atmospheric absorption bands in this spectral range are available for use in wavelength calibration.

[Title Page](#)[Abstract](#)[Introduction](#)[Conclusions](#)[References](#)[Tables](#)[Figures](#)[◀](#)[▶](#)[◀](#)[▶](#)[Back](#)[Close](#)[Full Screen / Esc](#)[Printer-friendly Version](#)[Interactive Discussion](#)

Nabro volcano aerosol in the stratosphere from twilight spectrometry

N. Mateshvili et al.

Title Page

Abstract

Introduction

Conclusions

References

Tables

Figures

◀

▶

◀

▶

Back

Close

Full Screen / Esc

Printer-friendly Version

Interactive Discussion

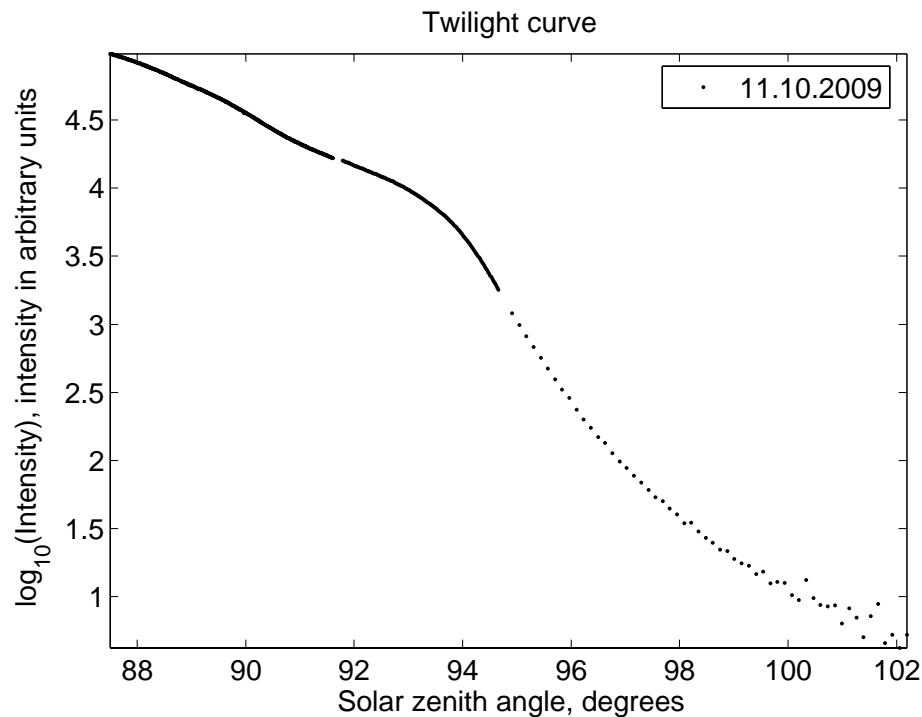


Fig. 4. An example of the measured twilight sky light intensity as a function of SZA. The curve is composed of three ensembles of consecutive measurements that differ in the exposure time. The gaps between the ensembles correspond to the interruptions needed to change the exposure time.

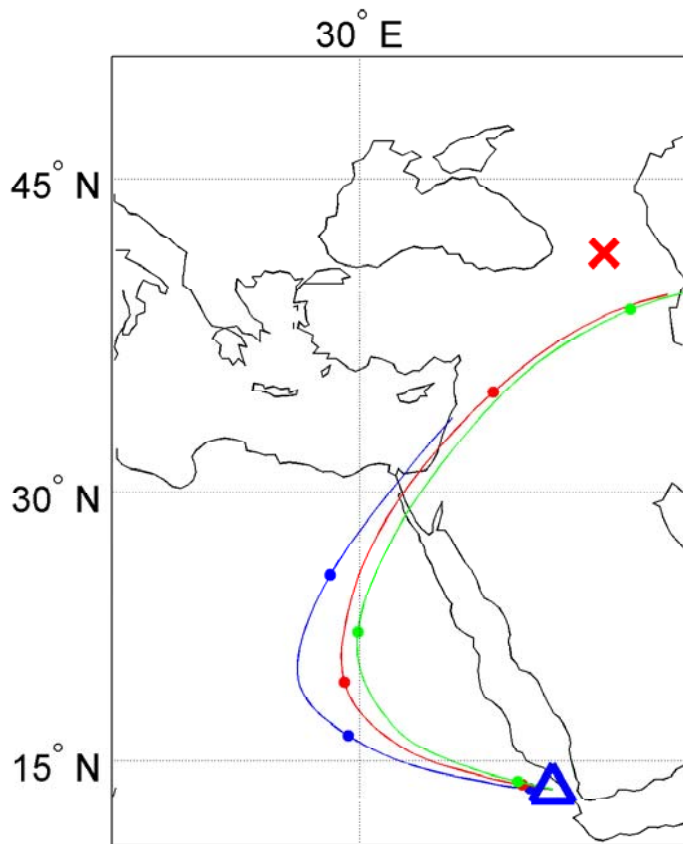


Fig. 5. Air parcel forward trajectories starting at altitudes 12 km (blue), 13 km (red) and 14 km (green) above the Nabro volcano (blue triangle) at the time of the eruption. Points on the trajectories mark the days after the eruption. The red cross marks the Tbilisi location.

Nabro volcano aerosol in the stratosphere from twilight spectrometry

N. Mateshvili et al.

Title Page	
Abstract	Introduction
Conclusions	References
Tables	Figures
◀	▶
◀	▶
Back	Close
Full Screen / Esc	
Printer-friendly Version	
Interactive Discussion	



Nabro volcano aerosol in the stratosphere from twilight spectrometry

N. Mateshvili et al.

Title Page

Abstract

Introduction

Conclusions

References

Tables

Figures

◀

▶

◀

▶

Back

Close

Full Screen / Esc

Printer-friendly Version

Interactive Discussion

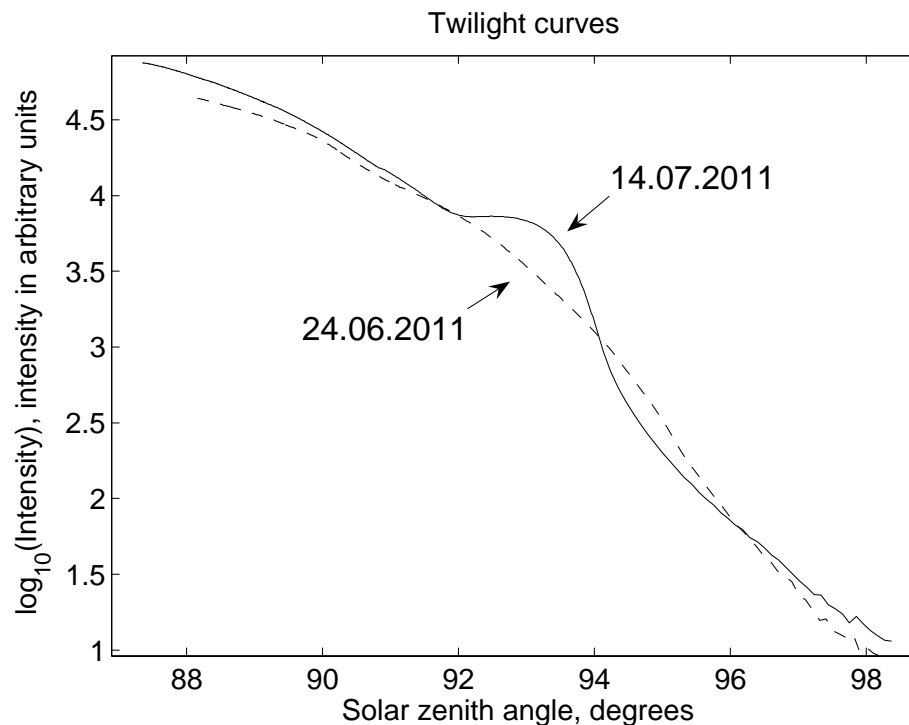


Fig. 6. A background twilight curve (dashed line, 24 June 2011) and one perturbed by volcanic aerosols after the June 2011 Nabro eruption (14 July 2011, solid line).

Nabro volcano
aerosol in the
stratosphere from
twilight spectrometry

N. Mateshvili et al.

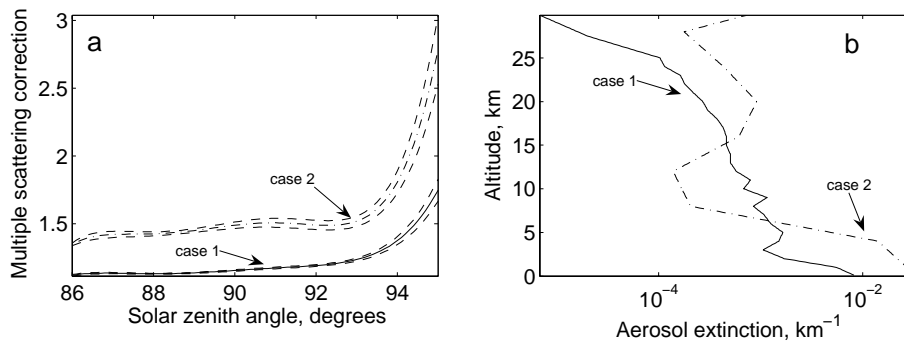


Fig. 7. (a) SZA dependences of multiple scattering correction factor (solid and dash-dotted line) for two cases of aerosol extinction profiles presented in panel (b). Dashed lines represent Monte Carlo uncertainties.

[Title Page](#)[Abstract](#)[Introduction](#)[Conclusions](#)[References](#)[Tables](#)[Figures](#)[◀](#)[▶](#)[◀](#)[▶](#)[Back](#)[Close](#)[Full Screen / Esc](#)[Printer-friendly Version](#)[Interactive Discussion](#)

Nabro volcano aerosol in the stratosphere from twilight spectrometry

N. Mateshvili et al.

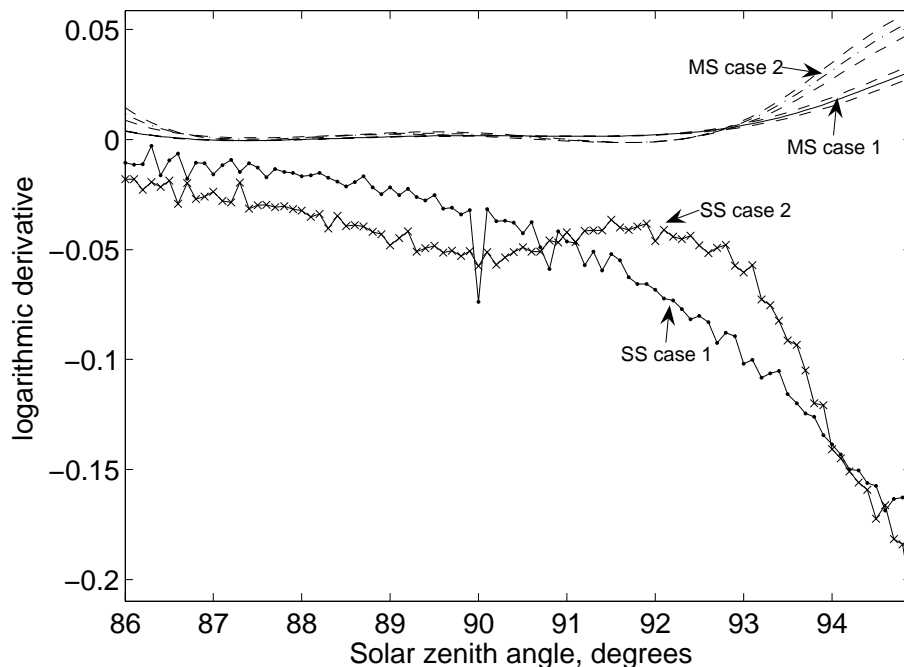


Fig. 8. Logarithmic derivatives for the single scattering (SS) intensities and multiple scattering (MS) corrections (solid and dash-dotted line) modeled by the Monte Carlo code for the two aerosol extinction profiles presented in Fig. 7b. $VZA = 45^\circ$. The multiple scattering correction curves are averaged over 10 Monte Carlo simulations and smoothed. The uncertainties of the multiple scattering contributions are shown by dashed lines.

[Title Page](#)[Abstract](#)[Introduction](#)[Conclusions](#)[References](#)[Tables](#)[Figures](#)[◀](#)[▶](#)[◀](#)[▶](#)[Back](#)[Close](#)[Full Screen / Esc](#)[Printer-friendly Version](#)[Interactive Discussion](#)

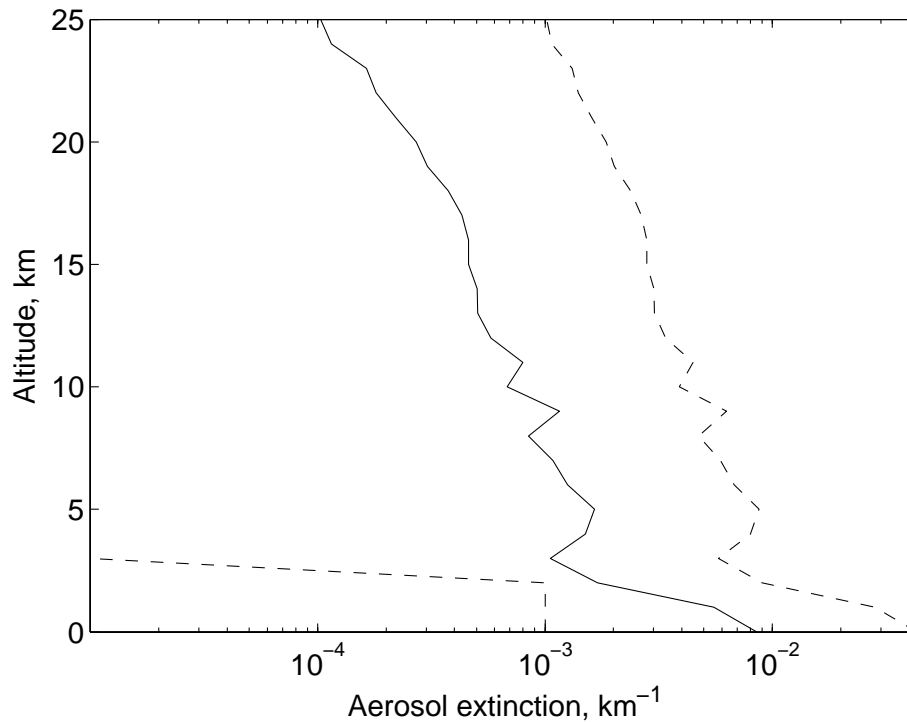


Fig. 9. The a priori state vector (solid line) with its uncertainties σ_a (dashed line).

Nabro volcano aerosol in the stratosphere from twilight spectrometry

N. Mateshvili et al.

Title Page

Abstract Introduction

Conclusions References

Tables Figures

⏪ ⏩

◀ ▶

Back Close

Full Screen / Esc

Printer-friendly Version

Interactive Discussion



Nabro volcano aerosol in the stratosphere from twilight spectrometry

N. Mateshvili et al.

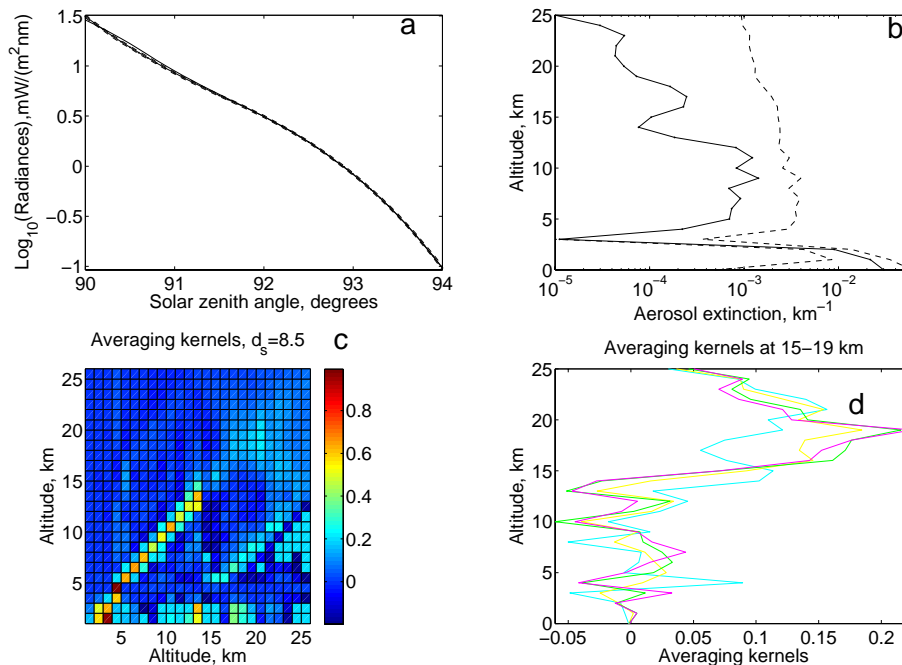


Fig. 10. Date of observation: 08 August 2010. **(a)** The measured twilight curve (solid dotted line) fitted by the modeled one (solid line) and measurement uncertainties (dashed lines). **(b)** The retrieved aerosol profile and corresponding uncertainty (dashed line); **(c)** averaging kernels, corresponding degree of freedom d_s is shown above the plot; **(d)** averaging kernels at altitudes 15–19 km.

[Title Page](#)
[Abstract](#)
[Introduction](#)
[Conclusions](#)
[References](#)
[Tables](#)
[Figures](#)
[◀](#)
[▶](#)
[◀](#)
[▶](#)
[Back](#)
[Close](#)
[Full Screen / Esc](#)
[Printer-friendly Version](#)
[Interactive Discussion](#)

Nabro volcano aerosol in the stratosphere from twilight spectrometry

N. Mateshvili et al.

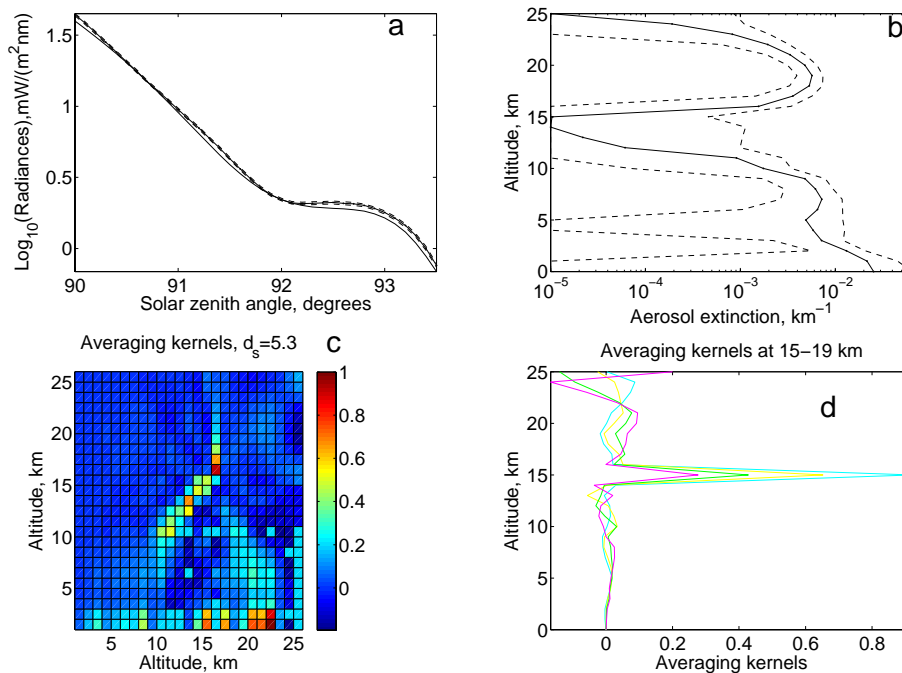


Fig. 11. Date of observation: 14 July 2011. Idem as Fig. 10.

Title Page

Abstract

Introduction

Conclusions

References

Tables

Figures

⏪

⏩

◀

▶

Back

Close

Full Screen / Esc

Printer-friendly Version

Interactive Discussion



Nabro volcano aerosol in the stratosphere from twilight spectrometry

N. Mateshvili et al.

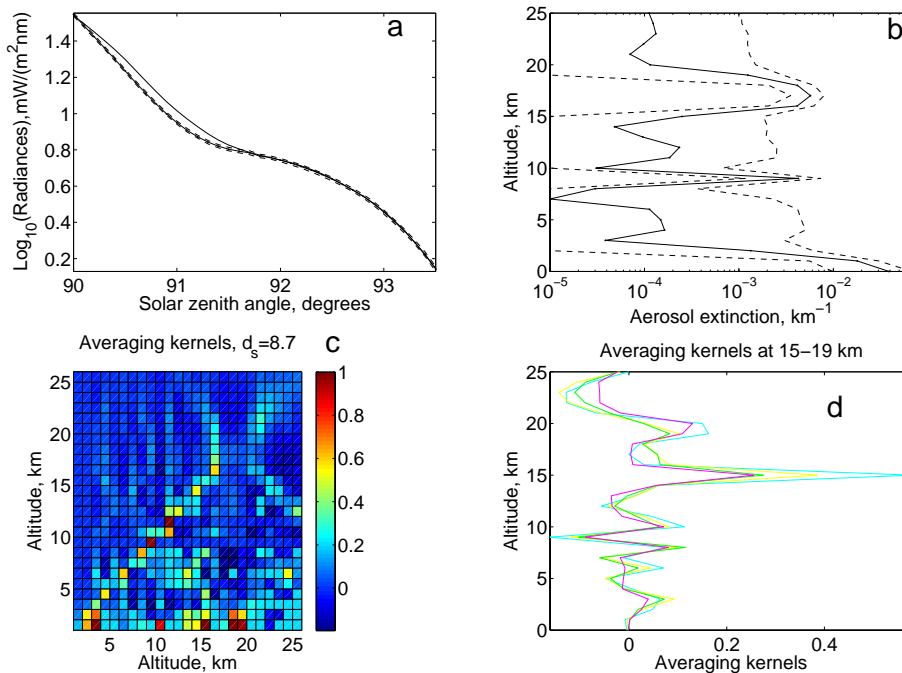


Fig. 12. Date of observation: 29 July 2011. Idem as Fig. 10.

Title Page

Abstract

Introduction

Conclusions

References

Tables

Figures

⏪

⏩

◀

▶

Back

Close

Full Screen / Esc

Printer-friendly Version

Interactive Discussion



Nabro volcano aerosol in the stratosphere from twilight spectrometry

N. Mateshvili et al.

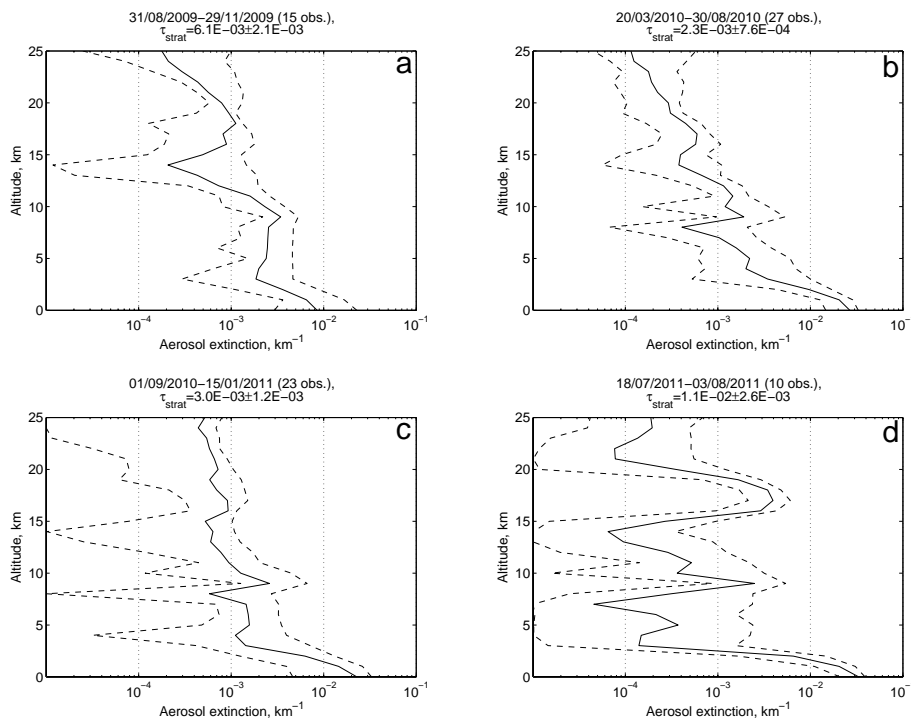


Fig. 13. 15.87%, 84.13% (dashed lines) and 50% (solid line) percentiles for the ensembles of retrieved aerosol extinction profiles. The period of data acquisition, number of observations and corresponding average stratospheric aerosol optical depth are indicated above the panels.

[Title Page](#)
[Abstract](#)
[Introduction](#)
[Conclusions](#)
[References](#)
[Tables](#)
[Figures](#)
[◀](#)
[▶](#)
[◀](#)
[▶](#)
[Back](#)
[Close](#)
[Full Screen / Esc](#)
[Printer-friendly Version](#)
[Interactive Discussion](#)

Nabro volcano aerosol in the stratosphere from twilight spectrometry

N. Mateshvili et al.

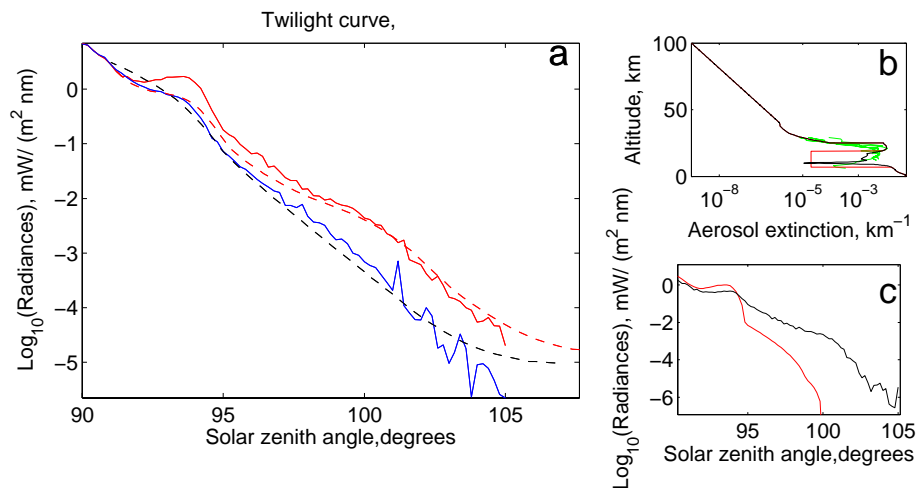


Fig. 14. (a) Twilight measurement acquired before (dashed black line) and after the Pinatubo eruption in 1991 (dashed red line). The solid blue curve was modeled using the aerosol profile shown in (b), black line, the solid red curve was modeled using the aerosol profile shown in (b), black line with red line correction. (b) The retrieved aerosol profile (solid black line), the correction (red line), SAGE II aerosol profiles (green lines). (c) The contribution of single (red) and double (black) scattering to the red modeled curve shown in (a).

[Title Page](#)
[Abstract](#)
[Introduction](#)
[Conclusions](#)
[References](#)
[Tables](#)
[Figures](#)
[⏪](#)
[⏩](#)
[◀](#)
[▶](#)
[Back](#)
[Close](#)
[Full Screen / Esc](#)
[Printer-friendly Version](#)
[Interactive Discussion](#)

Nabro volcano aerosol in the stratosphere from twilight spectrometry

N. Mateshvili et al.

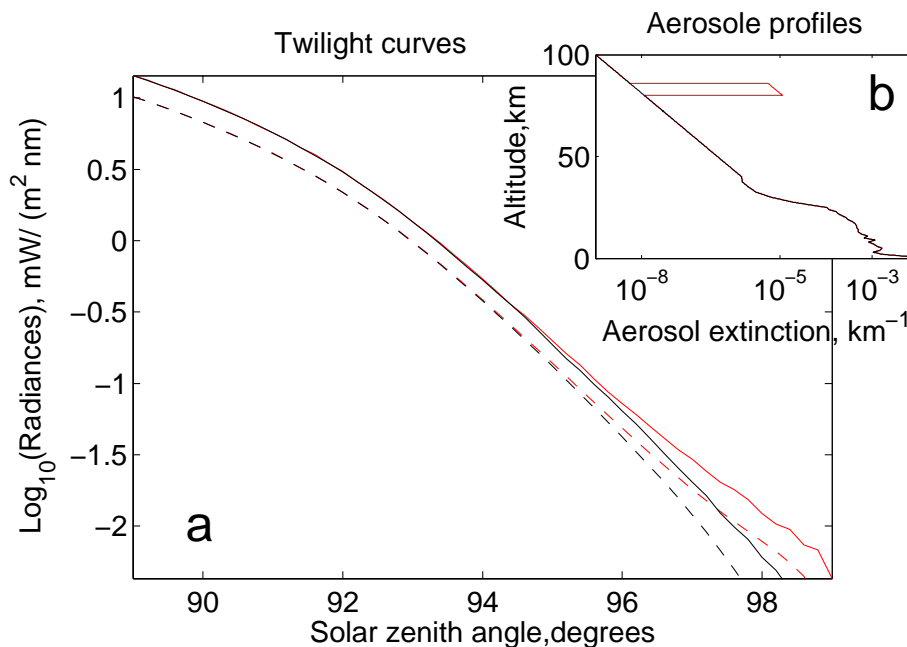


Fig. 15. The modeled twilight curves (solid lines) in case of absence (black) and presence (red) of a mesospheric aerosol layer (red line in **b**) with an extinction of 10^{-5} at 80–85 km. The corresponding single scattering is shown by dashed line. (**b**) Aerosol profile (black) used to model black curve in (**a**), red line – a mesospheric aerosol layer used to model red curve in (**a**).

Title Page

Abstract

Introduction

Conclusions

References

Tables

Figures

◀

▶

◀

▶

Back

Close

Full Screen / Esc

Printer-friendly Version

Interactive Discussion